Two-Phase Electronic Cooling Using Mini-Channel and Micro-Channel Heat Sinks: Part 2—Flow Rate and Pressure Drop Constraints

M. B. Bowers
Graduate Student.

I. Mudawar
Professor and Director.

Electronic Cooling Research Center,
Boiling and Two-Phase Flow Laboratory,
School of Mechanical Engineering,
Purdue University,
West Lafayette, IN 47907

Increased rate of heat dissipation from electronic chips was explored by the application of flow boiling in mini-channel ($D = 2.54$ mm) and micro-channel ($D = 510$ μm) heat sinks with special emphasis on reducing pressure drop and coolant flow rate. A pressure drop model was developed that accounts for the single-phase inlet region, the single- and two-phase heated region, and the two-phase unheated outlet region. Inlet and outlet losses associated with the abrupt contraction and expansion, respectively, were also accounted for, and so were the effects of compressibility and flashing within the two-phase region. Overall, the major contributor to pressure drop was the acceleration caused by evaporation in the channels; however, compressibility effects proved significant for the micro-channel geometry. Based upon practical considerations such as pressure drop, erosion, choking, clogging, and manufacturing ease, the mini-channel geometry was determined to offer inherent advantages over the micro-channel geometry. The latter is preferred only in situations calling for dissipation of high heat fluxes where minimizing weight and liquid inventory is a must.

Introduction

In the electronics industry, increased component concentration at the chip level has lead to significant increases in the chip cooling requirements due to greater dissipative heat fluxes. New technologies are in the development stages to meet these cooling demands, which include the Tuckerman and Pease (1981) micro-channel high flux heat sink. Flow in micro-channels has been demonstrated to yield very high single-phase heat transfer coefficients; however, this is achieved at the expense of an enormous pressure drop. An alternative to single-phase cooling is flow boiling, which offers the advantage of a lower flow rate for dissipating heat fluxes comparable to, or greater than those of micro-channel heat sinks.

A problem unique to flow boiling is the production of vapor bubbles that leads to increased pressure drop as compared to liquid flow; however, with the combination of lower flow rates and larger channel diameters, pressure drops can still be maintained lower than those with single-phase micro-channel flow. Several techniques are available for predicting two-phase pressure drop, and these techniques vary greatly in complexity and the method of determining void fraction and friction pressure drop. Zuber and Findlay (1965) accounted for the difference between the vapor and liquid velocities with a drift velocity in their drift-flux model which provided a powerful empirical technique for calculating void fraction. However, the drift-flux model requires prior knowledge of the two-phase flow patterns since a different drift velocity is used for each regime. Using a separated flow model, Lockart and Martinelli (1949) related the two-phase frictional pressure gradient to the purely liquid or vapor pressure gradients by friction multipliers whose magnitudes are dependent upon the mass quality. Other separated two-phase flow models are also available (e.g., Martinelli and Nelson, 1948; Thom, 1964) which employ correlation methods to determine the friction multiplier. For cases where the frictional and gravitational components of pressure drop are small in comparison with the accelerational component, the homogeneous equilibrium model (Wallis, 1969; Collier, 1981) offers a simple, yet fairly accurate, approach to calculating two-phase pressure drop. The homogeneous equilibrium model assumes the flow quality within the saturated region equal to the thermodynamic equilibrium quality. This model was employed for the two-phase pressure drop predictions of the present study.

In Part 1 of this study (Bowers and Mudawar, 1994), it was shown that flow boiling in both mini-channel ($D = 2.54$ mm) and micro-channel ($D = 0.51$ mm) heat sinks is a technology capable of achieving high heat fluxes for electronic cooling applications with the advantages of low flow rate and low pressure drop. To optimize the design of a heat sink for a particular cooling application, an accurate analytical model

Contributed by the Electrical and Electronic Packaging Division for publication in the JOURNAL OF ELECTRONIC PACKAGING. Manuscript received by the EEPD January 1, 1994; revised manuscript received April 30, 1994. Associate Technical Editor: B. G. Sammakia.

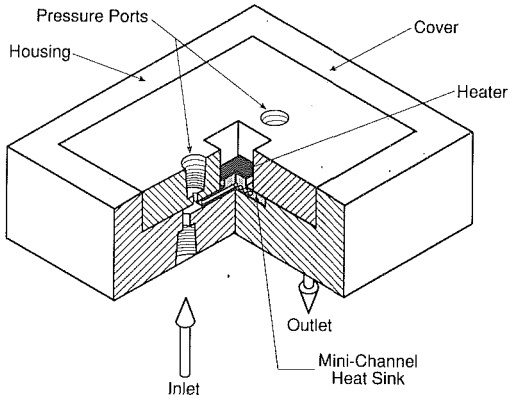

Fig. 1 Test module

for predicting pressure drop is needed. In this paper, a pressure drop model is presented, and its results are compared with experimental data that were obtained using the test module shown in Fig. 1, which is described in detail in another paper by Bowers and Mudawar (1994). Test cases are then compared to ascertain the major parameters influencing the pressure drop in two-phase miniature heat sinks. Also, an example is presented to clearly illustrate the use of the complete two-phase heat sink design package, which is the analytical tools presented in this paper for predicting pressure drop combined with those presented in Part 1 of the study for channel spacing and heat sink thickness.

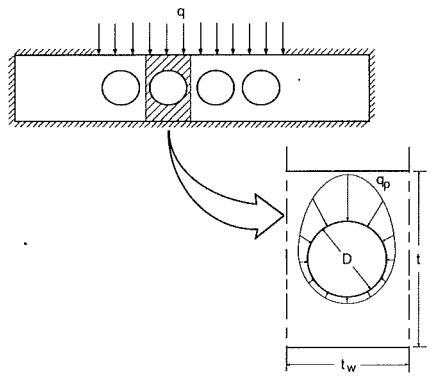

Fig. 2(a)

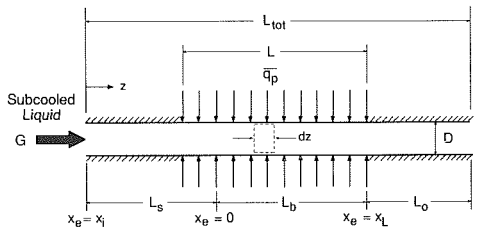

Fig. 2(b)

Fig. 2 Schematic of mini- or micro-channel heat sink geometry illustrating (a) nonuniform heat flux, q_p, along the channel perimeter for a uniform heat flux, q, applied along the upper surface; and (b) nomenclature used in the pressure drop model for a subcooled inlet

Pressure Drop Model

When designing a cooling scheme, the diameter and flow rate must be chosen not only to dissipate the heat load and prevent CHF but also to minimize pressure drop. This requires the development of analytical tools for the prediction of pressure drop. To meet this design need, a pressure drop model for a mini- or micro-channel heat sink was developed that includes both the single-phase and two-phase regions and accounts for compressibility and flashing within the two-phase region.

As shown in Fig. 2(*a*), a uniform heat flux applied at the upper surface of the heat sink yields a non-uniform heat flux, q_p, along the channel circumference whose mean value is

$$\overline{q_p} = \frac{1}{\pi D}\int_0^{\pi} q_p(\theta) D\, d\theta. \tag{1}$$

Nomenclature

c_p = specific heat at constant pressure
D = channel diameter
f = friction factor
f_s = Fanning friction factor
f_{TP} = two-phase friction factor
G = mass velocity, $4\rho_f Q_T/(N\pi D^2)$
h = enthalpy
h_{fg} = latent heat of vaporization
K = loss coefficient
L = heated length of heat sink channel
L_b = boiling length of channel's heated section
L_{ent} = entrance length for laminar boundary layer development
L_o = outlet length of heat sink channel
L_s = length of channel's inlet single-phase region
L_{tot} = total length of channel
M = two-phase Mach number
N = number of channels in heat sink
P = pressure
ΔP = pressure drop
q = heat flux based upon 1-cm^2 heated upper surface of heat sink
q_p = local heat flux along the channel inside area
$\overline{q_p}$ = mean heat flux based upon channel inside area
Q_T = total volumetric flow rate of heat sink
Re_D = Reynolds number based upon channel diameter, GD/μ_f
t = thickness of heat sink
ΔT_{sub} = liquid subcooling at channel inlet
t_w = width of cross-sectional cell containing one channel
U = mean velocity, $(v_f + xv_{fg})G$
v = specific volume
v_{fg} = difference in specific volumes of saturated vapor and saturated liquid
x = mass vapor quality; $x = 0$ for $x_e < 1$, $x = x_e$ for $0 < x_e < 1$, $x = 1$ for $x_e > 1$
x_e = thermodynamic equilibrium quality
x_i = equilibrium quality at the channel inlet
x_L = equilibrium quality at the end of the heated length
z = coordinate in flow direction
α = void fraction
θ = circumferential coordinate
μ = dynamic viscosity
ρ = density
τ = shear stress

Subscripts

b = boiling length
c = contraction
d = fully developed boundary layer
e = expansion
exp = experimental
f = liquid
g = vapor
i = inlet
max = maximum
o = outlet
p = channel perimeter (inside area), plenum
pred = predicted
ref = reference
u = developing boundary layer
2ϕ = two phase

Figure 2(*b*) shows the channel total length, L_{tot}, consists of a middle heated section of length L as well as unheated inlet and outlet lengths. For convenience in predicting the pressure drop, the total length is divided into three sections based upon the boundary conditions and the range of thermodynamic equilibrium quality, x_e. From the subcooled inlet ($x_i < 0$) to the location of $x_e = 0$ is the single-phase length, L_s, which consists of both the unheated inlet and a portion of the heated section. The next section begins with a zero quality and continues to the end of the heated length ($x_e = x_L$), and is referred to as the boiling length, L_b, due to the net vapor production as a result of saturated boiling. The remainder of the channel is the outlet length, L_o, which is unheated and characterized by a fairly constant value of quality ($x_e \approx x_L$). The pressure drop calculations for each of the three sections will be discussed beginning with the two-phase pressure drop of the boiling length.

Two-Phase Pressure Gradient. The boiling length ($0 < x_e < x_L$) is characterized by saturated boiling that produces a net vapor generation resulting in an increase in pressure drop as compared to purely liquid flow. Using the homogeneous equilibrium model, the liquid and vapor phases are assumed to form a homogeneous mixture with equal and uniform velocities, and properties are assumed to be uniform within each phase. Equilibrium flow indicates that the phases are in thermal equilibrium, and property values for the liquid and vapor phases are the saturated values based upon the local pressure.

Writing a mass balance for the differential control volume shown in Fig. 2(*b*) yields

$$\frac{d}{dz}\left(\frac{\pi D^2}{4}G\right) = 0, \tag{2}$$

which amounts to a constant mass velocity since the flow area is constant.

The local enthalpy, h, within the saturated region can be expressed as

$$h = h_f + x_e h_{fg}, \tag{3}$$

where h_f and h_{fg} are the local liquid enthalpy and latent heat of vaporization, respectively. Accounting for changes in kinetic energy and assuming negligible potential energy changes, conservation of energy for the control volume shown in Fig. 2(*b*) yields

$$\pi D\overline{q_p} = G\frac{\pi D^2}{4}\frac{d}{dz}\left(h + \frac{U^2}{2}\right) = G\frac{\pi D^2}{4}\frac{d}{dz}\left(h_f + x_e h_{fg} + \frac{1}{2}(v_f + x_e v_{fg})^2 G^2\right), \tag{4}$$

where U is the local mean mixture velocity.

Neglecting gravitational effects and accounting for friction and acceleration, a momentum balance on the control volume leads to

$$-\left(\frac{dP}{dz}\right)\frac{\pi D^2}{4} = \pi D\frac{f_{TP}U^2}{2(v_f + x_e v_{fg})} + G\frac{\pi D^2}{4}\left(\frac{dU}{dz}\right), \tag{5}$$

where P is the local pressure and f_{TP} is the two-phase friction factor. Expressing velocity in terms of mass velocity and mixture specific volume simplifies Eq. (5) to

$$-\left(\frac{dP}{dz}\right) = G^2\left[\frac{2}{D}f_{TP}(v_f + x_e v_{fg}) + \frac{d}{dz}(v_f + x_e v_{fg})\right]. \tag{6}$$

Assuming the properties within the saturated region ($0 < x_e < 1$) are functions of only the local pressure, Eq. (4) becomes

$$\frac{dx_e}{dz} = \frac{\frac{4\overline{q_p}}{GD} + \left[G^2(v_f + x_e v_{fg})\left(\frac{dv_f}{dP} + x_e\frac{dv_{fg}}{dP}\right) + \left(\frac{dh_f}{dP} + x_e\frac{dh_{fg}}{dP}\right)\right]\left(-\frac{dP}{dz}\right)}{h_{fg} + G^2(v_f + x_e v_{fg})v_{fg}}. \tag{7}$$

The above equation accounts for axial changes in quality due to heat input as well as flashing, that results from enthalpy changes with pressure, and compressibility, which is caused by changes in specific volume with pressure. In a similar manner, the pressure gradient of Eq. (6) is rearranged to account for property variations with pressure.

$$-\left(\frac{dP}{dz}\right) = \frac{\left(\frac{2f_{TP}G^2 v_f}{D}\right)\left[1 + x_e\left(\frac{v_{fg}}{v_f}\right)\right] + G^2 v_{fg}\frac{dx_e}{dz}}{1 + G^2\left(\frac{dv_f}{dP} + x_e\frac{dv_{fg}}{dP}\right)}. \tag{8a}$$

The numerator in Eq. (8*a*) is the sum of the frictional and accelerational pressure gradients. The former varies with flow quality while the accelerational gradient varies with the quality gradient. Incorporating Eq. (7) into the pressure gradient and rearranging yields

$$-\left(\frac{dP}{dz}\right) = \frac{\left(\frac{2f_{TP}G^2 v_f}{D}\right)\left[1 + x_e\left(\frac{v_{fg}}{v_f}\right)\right] + \frac{4\overline{q_p}Gv_{fg}}{D\left(h_{fg} + G^2 v_{fg}(v_f + x_e v_{fg})\right)}}{1 + G^2\left(\frac{dv_f}{dP} + x_e\frac{dv_{fg}}{dP}\right)\left[1 - \frac{G^2 v_{fg}(v_f + x_e v_{fg})}{h_{fg} + G^2 v_{fg}(v_f + xv_{fg})}\right] - \left[\frac{G^2 v_{fg}\left(\frac{dh_f}{dP} + x_e\frac{dh_{fg}}{dP}\right)}{h_{fg} + G^2 v_{fg}(v_f + xv_{fg})}\right]} \tag{8b}$$

In addition to the frictional and accelerational components in the numerator of Eqs. (8*a*) and (8*b*), the denominator of Eq. (8*b*) can be expressed as $1 - M^2$, where M is the two-phase Mach number. The Mach number expression accounts for not only compressibility effects but also kinetic energy and flashing as a result of property variations with pressure. Equations (7) and (8*a*) are coupled differential equations which are solved simultaneously to determine the two-phase pressure drop, ΔP_b, of the channel's heated section within the saturated region ($0 < x_e < 1$) as well as the pressure drop of the unheated outlet length, ΔP_o.

Single-Phase Pressure Drop. For the inlet region of the channel there is a developing velocity boundary layer up to the location where the wall effect is felt at the channel centerline yielding a fully developed velocity profile. Therefore, the single-phase flow is broken into two regions depending upon the flow conditions. For the range of velocities

covered in the present study, the flow remains in the laminar regime ($Re_D < 2300$), thus the entrance length (Langhaar, 1942),

$$L_{ent} = 0.05\,Re_D D. \tag{9}$$

For axial locations within the entrance length, the developing boundary layer is similar to that for flow over a flat plate. This assumption allows prediction of the pressure drop $\Delta P_{i,u}$, for the developing region from the Blasius solution (Schlichting, 1955) as

$$\Delta P_{i,u} = \frac{2.66\ G^{1.5}}{\rho_f D}\,(\mu_f z)^{0.5}, \tag{10}$$

where z is the shortest of L_{ent} or L_s. For the remaining single-phase region (assuming $L_s > L_{ent}$), the flow is fully developed, and the pressure drop is

$$\Delta P_{i,d} = \frac{2f_s G^2 (L_s - L_{ent})}{\rho_f D}, \tag{11}$$

where $f_s = 16/Re_D$ for laminar flow. The total pressure drop for the single-phase inlet region is calculated as

$$\Delta P_i = \Delta P_{i,u} + \Delta P_{i,d}. \tag{12}$$

Contraction and Expansion Pressure Drops. Associated with the abrupt contraction and expansion at the channel's inlet and outlet are the respective pressure drops ΔP_c and ΔP_e, which are the form and acceleration or deceleration losses (Todreas and Kazimi, 1990). These pressure drops are calculated as

$$\Delta P_c = \frac{1}{2v_f}\left(U_i^2 - U_{p,i}^2\right) + \frac{K_c}{2v_f}U_i^2, \tag{13}$$

and

$$\Delta P_e = \frac{1}{2(v_f + xv_{fg})}\left(U_{p,o}^2 - U_o^2\right) + \frac{K_e}{2(v_f + xv_{fg})}\left(U_o^2\right), \tag{14}$$

where U_i and U_o are the channel inlet and outlet velocities, and $U_{p,i}$ and $U_{p,o}$ are the velocities in the inlet and outlet plenums, respectively. K_c and K_e are the loss coefficients for the abrupt contraction and expansion, respectively, whose values for the present geometry are close to unity.

Comparison With Experimental Data. A complete expression for the pressure drop of the mini- or micro-channel heat sink is

$$\Delta P = \Delta P_c + \Delta P_i + \Delta P_b + \Delta P_o + \Delta P_e, \tag{15}$$

where ΔP_c, ΔP_i, ΔP_b, ΔP_o, and ΔP_e are determined from Eqs. (7) through (14). For the ΔP_b prediction, Eqs. (7) and (8a) were solved simultaneously using a Runge-Kutta technique. The same technique was employed to evaluate the outlet pressure drop, ΔP_o, using Eqs. (7) and (8a), after setting $\overline{q_p} = 0$. A comparison of the predicted pressure drop with experimental data is shown in Fig. 3. The plot includes data for both the mini- and micro-channel heat sinks for which $x_L < 1$; however, most are for the micro-channel due to its broader range of pressure drop. The value of $f_{TP} = 0.003$ was used since this value is recommended for applications involving flashing low-pressure flows (Collier, 1981). The usefulness of the model as a predictive tool is clearly illustrated by the plot with most data points falling within a $+/-$ 30 percent error band.

Compressibility and Flashing Effects. To make greater use of the pressure drop model, three test cases were analyzed to examine the development of key flow parameters with respect to axial location for both the mini- and micro-channel heat sinks. This analysis was aimed at evaluating the individual contributions of these parameters to the total pressure drop. For the test cases, a very low flow rate of $Q_T = 26$ ml min^{-1} and a high value of 64 ml min^{-1} were chosen, the latter being the highest flow rate experimentally tested for both heat sinks. Uniform heat flux values of $q = 100$ and 200 W cm^{-2} were used with all cases, representing values for high flux electronic cooling applications.

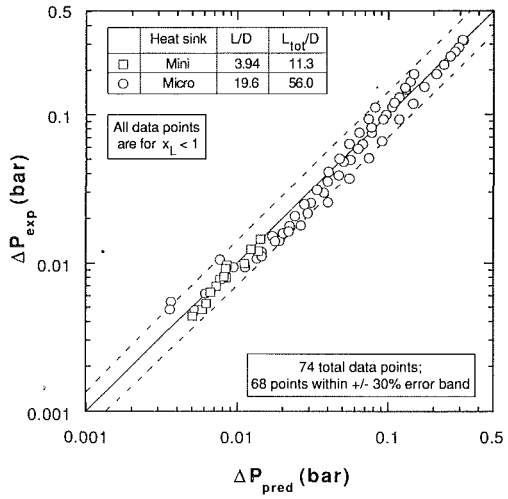

Fig. 3 Comparison of predictions of pressure drop model with experimental data

Figures 4(a) and 4(b) show numerical predictions of equilibrium quality, x_e, and pressure for the mini-channel and micro-channel heat sinks, respectively. Also shown is the void fraction, α, as predicted from the homogeneous equilibrium model. α assumes the values 0 and 1 for $x_e < 0$ and $x_e > 1$, respectively, and, in the saturated region ($0 < x_e < 1$),

$$\alpha\rho_g + (1-\alpha)\rho_f = \frac{1}{x_e v_g + (1-x_e)v_f}. \tag{16}$$

Rearranging Eq. (16) yields an expression for α applicable to the saturated region.

$$\alpha = \frac{1}{1 + \left(\dfrac{1-x_e}{x_e}\right)\dfrac{\rho_g}{\rho_f}}. \tag{17}$$

For both heat sinks, the model predicts essentially no change in quality outside of the heated region and a linear rise in quality in the heated region. The slope of the quality curve is predominantly determined by the ratio of heat flux to mass velocity because the effect of total heat input on the change in quality is greater than the effect of flashing by several orders of magnitude. In contrast, there is an abrupt rise in void fraction to above 0.9 a very short distance downstream of the point of net vapor production ($x_e = 0$), proving a departure from the dispersed flow assumption of the homogeneous model to the separated annular flow regime is prevalent over most of the heated section. The implications of this departure will be discussed later. The corresponding pressure drops for the mini-channel are negligible, with the greatest (~ 0.02 bar) occurring in the heated section for test case C as a result of the greater heat input. The micro-channel test cases, Fig. 4(b), show very little pressure change within the single-phase region; however, there are considerable pressure losses associated with the two-phase heated section and outlet length. The distinctive offset between cases A and B, with total pressure drops of 0.025 and 0.07 bar, respectively, is due to the increase in mass velocity corresponding to the increase in total flow rate from A to B. The greatest pressure drop (~ 0.22 bar) resulted from the

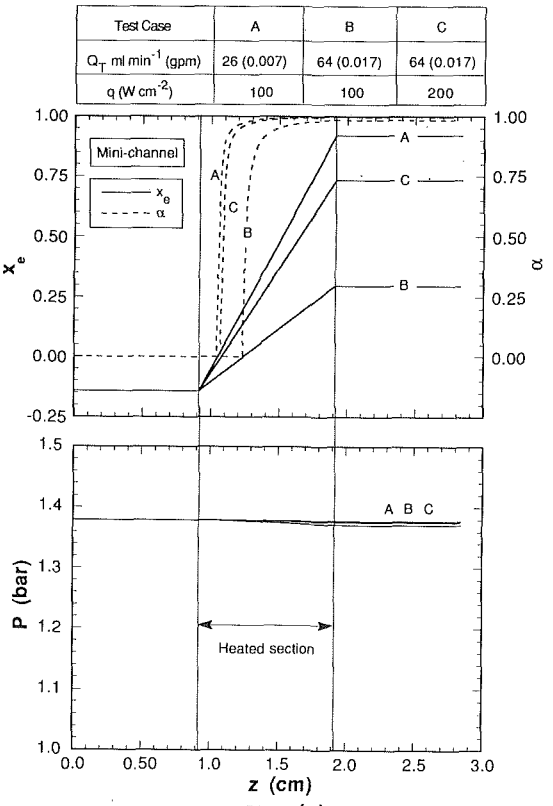

Fig. 4(a)

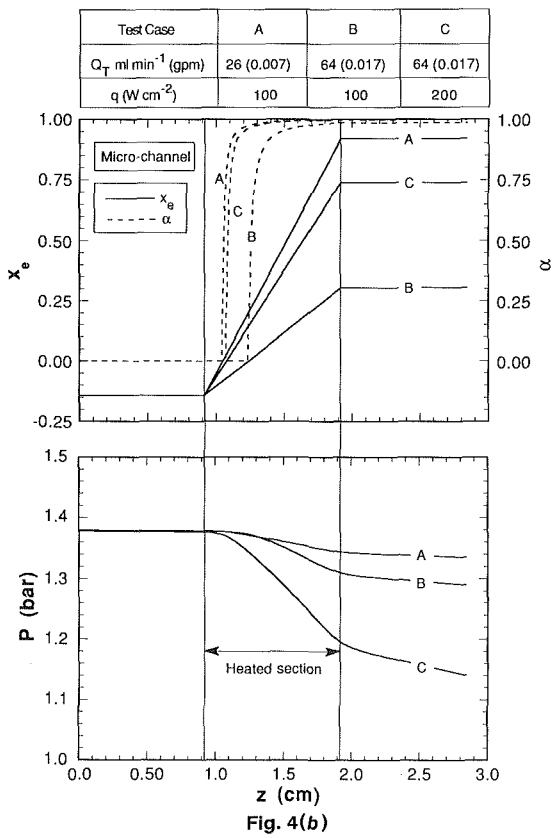

Fig. 4(b)

Fig. 4 Numerical predictions of quality, void fraction, and pressure for the (*a*) mini-channel heat sink and (*b*) micro-channel heat sink

combined effects of high flow rate and large heat input of case C. The pressure drop is greater than for case B as a result of greater acceleration losses associated with the increased quality gradient as indicated by the steeper slope of the corresponding quality curve. The effects of the two-phase mixture are also apparent in the unheated exit length, where friction is the predominant contributor to pressure drop, and the higher flow rate and higher quality of case C combined to yield a greater pressure drop.

The local mean velocity and two-phase Mach number are presented in Figs. 5(*a*) and 5(*b*) for the mini-channel and micro-channel heat sinks, respectively. For the mini-channel heat sink, the velocity increases in the heated section as a result of a reduction in average density that accompanies the vapor production; however, the velocity remains at a reasonable level of less than 8 m s^{-1} even at the highest flow rate. Compressibility effects are negligible for the mini-channel as indicated by the Mach numbers remaining below 0.09. In contrast, the micro-channel acquires a very large increase in velocity, Fig. 5(*b*), within the heated section, especially for case C. The mean velocity for this case increases from below 0.05 to 40 m s^{-1} as a result of the reduction in average density combined with the small flow area of the micro-channel heat sink. This acceleration is responsible for the large pressure drop within the heated section. Compressibility is also a contributor to the pressure losses as indicated in the Mach number plot. For case C, the Mach number increases to 0.42 at the end of the heated length, and to 0.44 in the unheated outlet length. The property variations with pressure are also apparent in the velocity plot, explaining the continued increase in velocity in the unheated outlet length where quality is relatively constant. The Mach number plot clearly illustrates a problem associated with flow boiling in micro-channel heat sinks. Heat fluxes of magnitude not much greater than those of case C would lead to choking ($M = 1$). A condition of choked flow would result in a premature CHF which can be disastrous for electronic cooling. Also, based purely upon CHF calculations, cooling system failure due to choked flow is not predictable.

Figure 6(*a*) shows the change in latent heat of vaporization, h_{fg}, and liquid enthalpy, h_f, for a pressure range from 1.0 to 2.0 bar. The plot shows very little change in the latent heat of vaporization, which has a weak downward slop for the pressure range of the present study. The liquid enthalpy slopes upward with a little greater magnitude; however, as previously mentioned, the effect of flashing that results from these enthalpy changes with pressure is negligible in comparison to the total heat input. Figure 6(*b*) illustrates the specific volume changes for a corresponding change in absolute pressure from 1.0 to 2.0 bars. There is a negligible change in liquid specific volume, v_f, for the pressure range shown, which is in great contrast to the liquid-vapor specific volume difference, v_{fg}. It almost doubles in magnitude for a decrease in pressure from 2.0 to 1.0 bars with the curve exhibiting a greater change in slope (i.e., greater compressibility) with decreasing pressure. This curve clearly illustrates why compressibility effects can become a problem with large pressure changes, especially for the low pressure range around 1.0 bar.

The previous discussion reveals that the major contributor to the total pressure drop for both the mini- and micro-channel heat sinks is the acceleration in the heated section. The same conclusion can be drawn by examining the individual contributions of acceleration and friction to the total pressure gradient as shown in Figs. 7(*a*) and 7(*b*) for the mini-channel and micro-channel heat sinks, respectively. The mini-channel pressure gradient is linear within the heated section due to the linear rise in flow quality, but the micro-channel exhibits a nonlinear behavior. While the major contributor to the overall pressure gradient is the acceleration, compressibility, especially with the micro-channel heat sink, accounts for the added nonlinear behavior of the pressure gradient. It is for the reason that friction has such a minor influence on pressure drop that the homogeneous equilib-

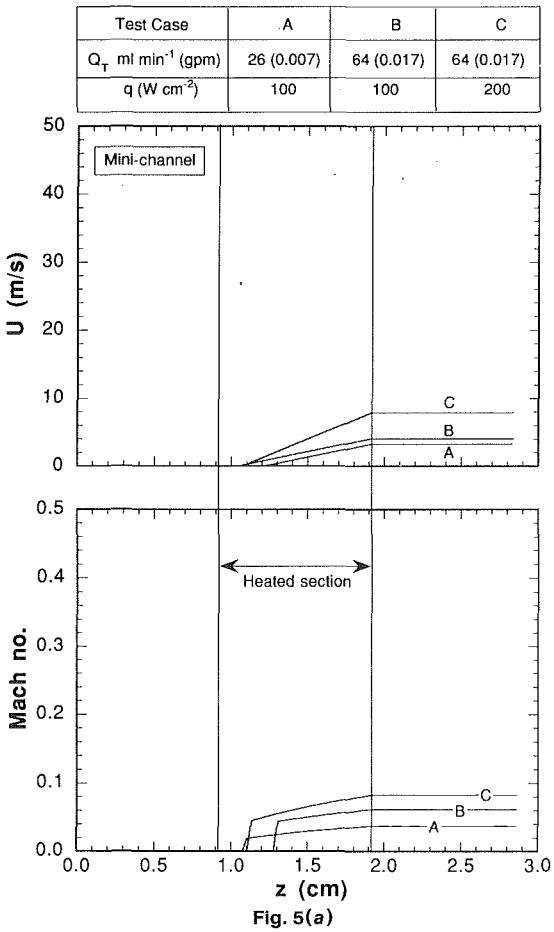

Fig. 5(*a*)

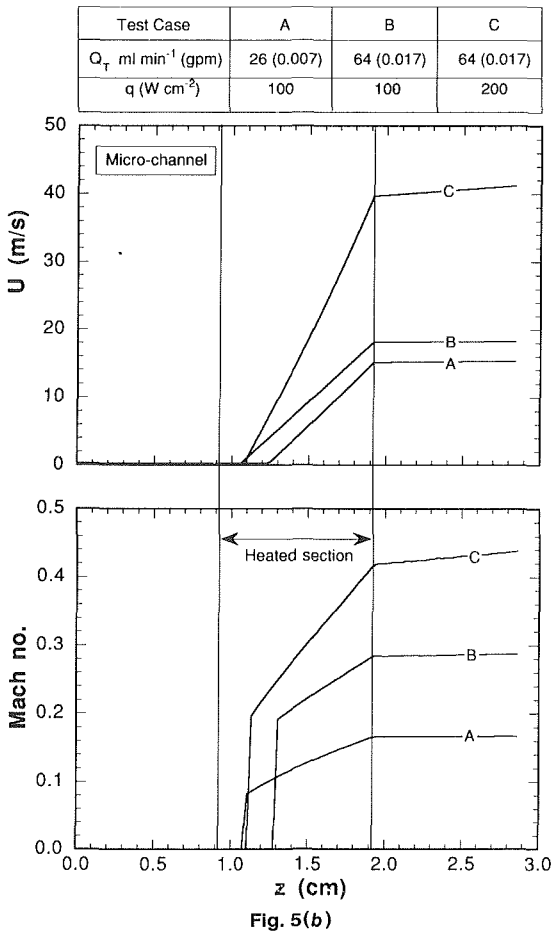

Fig. 5(*b*)

Fig. 5 Numerical predictions of mean velocity and two-phase Mach number for the (*a*) mini-channel heat sink and (*b*) micro-channel heat sink

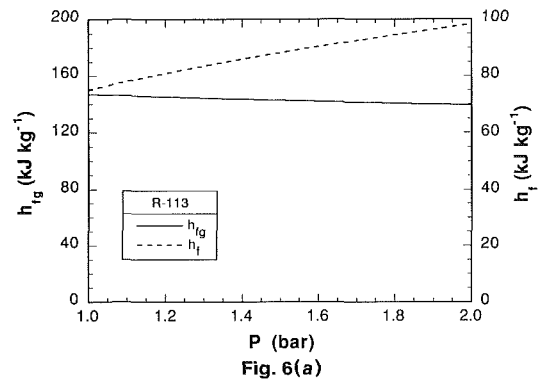

Fig. 6(*a*)

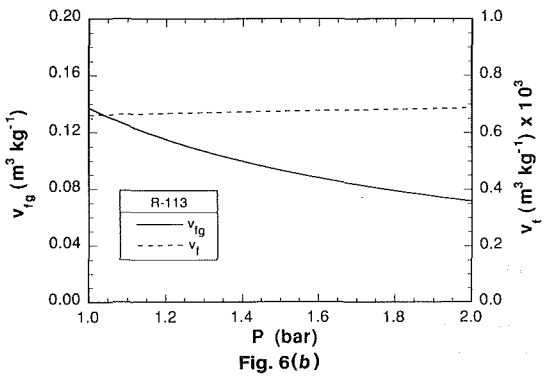

Fig. 6(*b*)

Fig. 6 Variations of (*a*) enthalpy and (*b*) specific volume with pressure

rium model is deemed appropriate for heat sink design. More advanced two-phase flow models (e.g., slip flow, drift flux, nonequilibrium flow) should improve the accuracy in describing the flow development in the channels, but not necessarily in predicting the pressure drop.

Since acceleration is the major contributor to pressure drop for miniature heat sinks, a simplified equation for predicting pressure drop can be found by assuming constant properties in Eqs. (7) and (8*a*) and neglecting the friction term of Eq. (8*a*). Integrating over the heated length yields

$$\Delta P = G^2 v_{fg} x_L \tag{18}$$

where

$$x_L = \frac{4\overline{q}_p L}{GDh_{fg}} - \frac{c_{p,f}\Delta T_{\text{sub}}}{h_{fg}} \tag{19}$$

where x_L is the thermodynamic equilibrium quality at the end of the heated section. Other factors that contribute to the pressure drop are compressibility, flashing, and kinetic energy changes associated with property variations; however, compressibility is the major contributor which can be estimated with the aid of a Mach number criterion. Referring to the denominator of Eq. (8*b*), changes in specific volume of liquid with pressure are negligible; therefore

$$M_{\max}^2 \cong -G^2 x_L \frac{\Delta v_{fg}}{\Delta P} \tag{20}$$

where ΔP is calculated from Eq. (18), and Δv_{fg} is the corresponding change in liquid-vapor specific volume difference determined from Fig. 6(*b*). A comparison of predicted

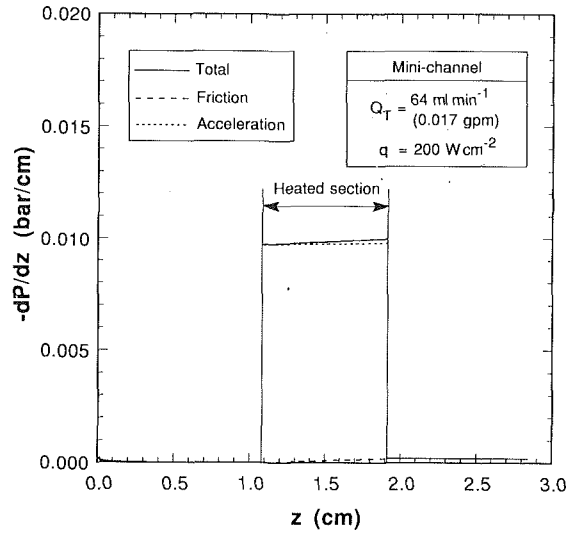

Fig. 7(*a*)

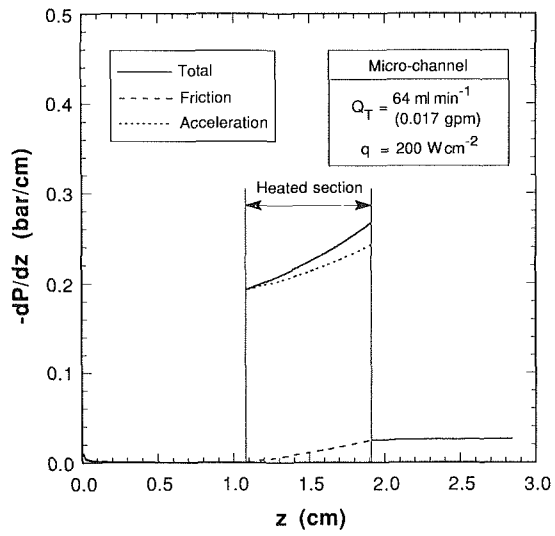

Fig. 7(*b*)

Fig. 7 Contributions of friction and acceleration total pressure gradient for (*a*) mini-channel heat sink and (*b*) micro-channel heat sink

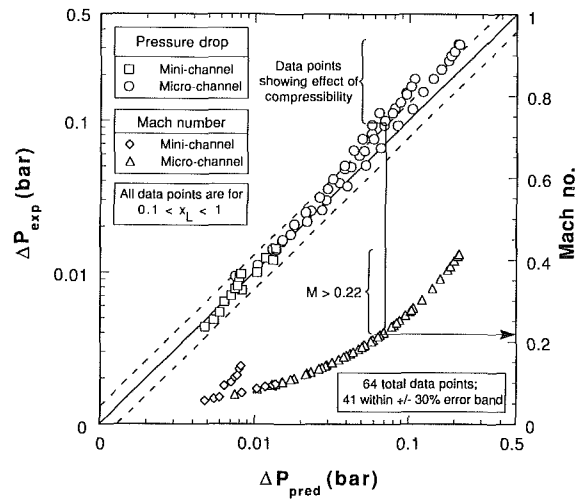

Fig. 8 Comparison of predictions of simplified acceleration pressure drop model with experimental data and corresponding two-phase Mach numbers

Table 1 Mini- and micro-channel heat sink performance based on a maximum heat flux of q = 400 W cm^{-2} and inlet pressure of 2.07 bar

Heat sink geometry	Q_T ml min^{-1} (gpm)	ΔP bar (psi)	M	$\tau_{2\phi}/\tau_{1\phi}$
Mini-channel D = 2.54 mm t_w/D = 1.3	190 (0.050)	0.021 (0.30)	0.13	0.90
Micro-channel D = 0.510 mm t_w/D = 1.15	142 (0.038)	0.63 (9.2)	0.66	2.60

pressure drop based upon Eq. (18) with experimental data is shown in Fig. 8, and also included on the plot are the corresponding Mach numbers determined from Eq. (20). The plot contains data for both the mini- and micro-channel heat sinks, and since the simplified model only accounts for acceleration pressure drop, the data is confined to cases where outlet equilibrium quality is greater than 0.1. All of the mini-channel data fall within a +/− 30 percent error band while micro-channel pressure drops above 0.08 bar begin to deviate, with pressures being less than the experimental values by more than 30 percent. For the higher pressure drops, compressibility effects cause a deviation from the experimental data which is evidenced by the corresponding rise in Mach number from 0.22 up to 0.4. Therefore, for a conservative prediction of pressure drop, it is advised that Eq. (20) be used to determine the Mach number in conjunction with the simple pressure drop prediction of Eq. (18), and for $M \gtrsim 0.22$, the complete pressure drop model should be used which accounts for compressibility effects as well as friction and flashing.

Applications of Design Methodology

In the Part 1 of the study (Bowers and Mudawar, 1994), cell width and thickness constraints were clearly established for an optimum heat sink design. The cell width and thickness requirements were $t_w/D < 2$ and $t/D = 1.2$ or smaller depending upon structural considerations. Diameter and flow rate are further determined based upon CHF and pressure drop criteria. The mini-channel and micro-channel geometries are compared to illustrate how these criteria can be utilized. It is assumed that, based upon heat transfer requirements and safety considerations, a maximum heat flux or CHF of 400 W cm^{-2} must be achieved. Using the CHF correlation given in Eq. (1) of Bowers and Mudawar (1994), this goal is met with a flow rate of 190 ml min^{-1} for the mini-channel and 142 ml min^{-1} for the micro-channel as given in Table 1. Corresponding pressure drop predictions are 0.021 and 0.63 bar for the mini- and micro-channel, respectively. Both heat sink geometries meet the thickness and cell width requirements; however, the advantage of a 25 percent reduction in coolant flow rate with the micro-channel is realized at the expense of an alarming 2900 percent increase in pressure drop. Both flow rates are very low compared to single-phase micro-channel heat sinks of comparable heat flux capability. The low flow rate requirement allowed the two-phase pressure drop of even the micro-channel heat sink to be smaller than that of single-phase microchannels; however, additional practical considerations should be addressed. The two-phase Mach number is negligible for the mini-channel in contrast with a value of M = 0.66 for the micro-channel. This result illustrates the high degree of compressibility possible with micro-channel heat sinks. An increase in flow rate for the micro-channel to achieve enhanced heat transfer performance or as a result of poor flow control would result in a much greater pressure drop and, possibly, choked flow. For the mini-channel, a similar in-

Table 2 Maximum allowable mean liquid velocity in internal flow for preventing erosion (Ayub and Jones, 1987)

Material	Water ($m\ s^{-1}$)	R-113* ($m\ s^{-1}$)
Low carbon steel	3.0	2.4
Stainless steel	4.6	3.7
Aluminum	1.8	1.5
Copper	1.8	1.5
90-10 cupronickel	3.0	2.4
70-30 cupronickel	4.6	3.7
Titanium	> 15	> 12

*Allowable velocity for water divided by (specific gravity)$^{1/2}$

crease in flow rate would not yield the same enhancement in thermal performance; however, practical problems such as pressure drop, choking, and clogging are not issues of concern with the mini-channel.

Erosion Considerations. Another issue which has great bearing on the practical implementation of the two-phase heat sinks in electronic cooling is channel erosion. The major cause of pressure drop in the two-phase heat sinks has been shown to be the acceleration associated with the large stream-wise increase in mean velocity. Accompanying the high velocities are shear stresses that may lead to channel erosion. For an approximation of the magnitude of wall shear stress, the two-phase shear stress is compared with that for single-phase flow at the upper erosion limit commonly imposed with metallic surfaces per Table 2 (Ayub and Jones, 1987). Assuming equal friction factors yields

$$\frac{\tau_{2\phi,\max}}{\tau_{1\phi,\mathrm{ref}}} = \frac{\left[f_{TP}\frac{1}{2}\frac{U^2}{(v_f + xv_{fg})}\right]_{\max}}{\left[f_s\frac{1}{2}\rho_f U^2\right]} = \frac{G^2(v_f + xv_{fg})}{\rho_f U^2}, \tag{21}$$

where $\tau_{2\phi,\max}$, $\tau_{1\phi,\mathrm{ref}}$, f_{TP}, and f_s are, respectively, the largest two-phase shear stress in the channel, the reference shear stress for single-phase flow at 1.5 m s^{-1} for the copper and 3.7 m s^{-1} for nickel (approximated from value for stainless steel), the two-phase friction factor, and the single-phase friction factor, and x is evaluated at the channel exit. Referring to Table 1, Eq. (21) predicts a micro-channel shear stress 2.6 times that of the reference case, compared to a shear stress ratio of 0.90 for the mini-channel. Erosion will, therefore, be within allowable limits for the mini-channel and beyond the practical design limits for the micro-channel at high heat fluxes.

It can clearly be concluded from the above example that, while both heat sinks can meet even the harshest of electronic cooling requirements, the mini-channel offers significant practical advantages. Low pressure drop, negligible compressibility, acceptible erosion, low likelihood of clogging, as well as manufacturing ease are all characteristics unique to the mini-channel geometry. Micro-channel heat sinks may be preferred only in situations demanding the dissipation of high heat fluxes and where minimizing weight and liquid inventory is a must (e.g., avionics and space electronics). The analytical tools presented in both this paper and Part 1 for determining channel spacing, pressure drop, Mach number, and erosion, coupled with the CHF correlation, constitute a comprehensive methodology for designing practical, high-flux cooling systems for electronic hardware.

Conclusions

A pressure drop model was developed to aid in optimizing the design of mini-channel and micro-channel heat sinks for electronic cooling. Key findings from the study are:

(1) The homogeneous equilibrium two-phase flow model is a fairly accurate tool for calculating the heat sink pressure drop, as well as a valuable method for analyzing the major parameters that affect the heat sink pressure drop.

(2) The major contributor to pressure drop for both the mini-channel and micro-channel is the acceleration resulting from evaporation; however, compressibility effects are significant for the micro-channel. Pressure drop in high-flux heat sinks can be predicted with reasonable accuracy by accounting for the accelerational pressure drop only; however, for cases where the Mach number exceeds 0.22, compressibility effects must also be considered to yield reliable predictions. Large pressure drop and the potential for choking warrant the use of channel diameters no smaller than the micro-channel (D = 510 μm) for high flux applications.

(3) Channel erosion due to flow boiling in the mini-channel geometry is less than that associated with maximum allowable limits for single-phase cooling; however, erosion effects associated with the micro-channel geometry are greater than the allowable limits at high heat fluxes.

Acknowledgment

The authors thank Mr. Kenneth Thompson of 3M Industrial and Electronics Sector Laboratories for providing the micro-channel heat sink for the present study.

References

Ayub, Z. H., and Jones, S. A., 1987, "Tubeside Erosion/Corrosion in Heat Exchangers," *Heating, Piping and Air Conditioning*, Vol. 59, pp. 81–82.

Bowers, M. B., and Mudawar, I., 1994, "Two-Phase Electronic Cooling Using Mini-channel and Micro-channel Heat Sinks—Part 1. Design Criteria and Heat Diffusion Constraints," ASME JOURNAL OF ELECTRONIC PACKAGING, Vol. 116, pp. 290–297.

Collier, J. G., 1981, *Convective Boiling and Condensation*, McGraw-Hill, London, pp. 26–35.

Incropera, F. P., and DeWitt, D. P., 1985, *Fundamentals of Heat and Mass Transfer*, Wiley, New York.

Langhaar, H. L., 1942, "Steady Flow in the Transition Length of a Straight Tube," ASME *Journal of Applied Mechanics*, Vol. 19, pp. A-55–A-58.

Lockart, R. W., and Martinelli, R. C., 1949, "Proposed Correlation of Data for Isothermal Two-Phase, Two-Component Flow in Pipes," *Chemical Engineering Progress*, Vol. 45, pp. 39–48.

Martinelli, R. C., and Nelson, D. B., 1948, "Prediction of Pressure Drop During Forced-Circulation Boiling of Water," *Trans. ASME*, Vol. 70, pp. 695–702.

Schlichting, H., 1955, *Boundary Layer Theory*, McGraw-Hill, New York, pp. 22–25.

Thom, J. R. S., 1964, "Prediction of Pressure Drop During Forced Circulation Boiling of Water," *International Journal of Heat and Mass Transfer*, Vol. 7, pp. 709–724.

Todreas, N. E., and Kazimi, M. S., 1990, *Nuclear Systems I*, Hemisphere, New York, pp. 398–403.

Tuckerman, D. B., and Pease, R. F. W., 1981, "High-Performance Heat Sinking for VLSI," *IEEE Electron Device Letters*, Vol. EDL-2, pp. 126–129.

Wallis, G. B., 1969, *One-Dimensional Two-Phase Flow*, McGraw-Hill, New York, pp. 17–35.

Zuber, N., and Findlay, J. A., 1965, "Average Volumetric Concentration in Two-Phase Flow Systems," ASME *Journal of Heat Transfer*, Vol. 87, pp. 453–468.